ISBN: 978-3-95450-232-5 ISSN: 2673-7000 doi:10.18429/JACoW-NAPAC2022-WEXD2

STORAGE RING TRACKING USING GENERALIZED GRADIENT REPRESENTATIONS OF FULL MAGNETIC FIELD MAPS*

R. Lindberg, M. Borland, ANL, Argonne, IL, USA

Abstract

We have developed a set of tools to simulate particle dynamics in the full magnetic field using the generalized gradients representation. Generalized gradients provide accurate and analytic representations of the magnetic field that allow for symplectic tracking. We describe the tools that convert magnetic field data into generalized gradients representations suitable for tracking in `elegant`, and discuss recent results based upon tracking with the full field representations for all magnets in the APS-U storage ring.

PREPARING THE GENERALIZED GRADIENT EXPANSION FOR `ELEGANT`

It has long been known that symplectic integration is important for long-term tracking in storage rings. Symplectic dynamics requires the divergence of the field to vanish, $\boldsymbol{\nabla}\cdot\boldsymbol{B}=0$, or in other words means that the magnetic field must be derivable from a vector potential $\boldsymbol{A}$. While this may not be an issue theoretically, it does pose a problem when one wants to use magnetic field data obtained from either measurements or simulation programs such as `OPERA`. In this case the quality of the data is not only limited by measurement or numerical precision, but also by the finite grid on which the values of $\boldsymbol{B}$ are known. At first glance it is not obvious how to interpolate the magnetic field to an arbitrary point in a way that satisfies Maxwell's equations, much less how to do this in a numerically optimal manner.

Fortunately, Dragt and collaborators have worked out most of these issues by introducing the generalized gradient representation of the magnetic field (see, e.g., [1–3]). The first important point is that the generalized gradient expansion gives a Taylor-series representation of the magnetic field anywhere in the transverse (x, y) plane at a sequence of longitudinal (z) coordinates. The resulting magnetic field is derivable from a vector potential, and therefore is divergence-free and suitable for symplectic tracking. Furthermore, the $\boldsymbol{B}$-field satisfies the source-free Ampère's law $\boldsymbol{\nabla}\times\boldsymbol{B}=0$ up to the order of the Taylor series.

The second important point is that the generalized gradient expansion is determined using only the field values on the boundary of a surface. Since both the "true" magnetic field and the numerically determined one satisfy $\boldsymbol{\nabla}^2\boldsymbol{B}=0$, their difference achieves its maximum value on the boundary. In other words, in the interior the difference between the "true" and calculated field is everywhere smaller than its largest value on the boundary.

In more concrete terms, we note that in free space the magnetic field can be described by either the vector potential via $\boldsymbol{B}=\boldsymbol{\nabla}\times\boldsymbol{A}$ or the scalar potential $\boldsymbol{B}=\boldsymbol{\nabla}\psi$; the latter can be expanded in terms of the generalized gradients as the following power series [3]:

$$\psi=\sum_{\ell=0}^{\infty}\sum_{m=1}^{\infty}\frac{(-1)^{\ell}m!}{2^{2\ell}\ell!(\ell+m)!}(x^2+y^2)^{\ell} \times\left\{C_{m,s}^{[2\ell]}(z)\Im(x+iy)^m+C_{m,c}^{[2\ell]}(z)\Re(x+iy)^m\right\}. \tag{1}$$

Here, $C_{m,s}(z)$ is the "sine-like" generalized gradient that gives the usual multipole of order m, while $C_{m,s}^{[2\ell]}$ is its $2\ell^{\text{th}}$ derivative with respect to z. The $C_{m,c}^{[2\ell]}$ are the "cosine-like" generalized gradients that give rise to skew components in the field. As another example relevant to tracking, the longitudinal component of the vector potential is

$$A_z(x,y,z)=-xC_{1,s}(z)-(x^2-y^2)C_{2,s}(z) -(x^3-3xy^2)C_{3,s}(z)+\ldots, \tag{2}$$

where C_1, C_2, and C_3 are the on-axis dipole, quadrupole, and sextupole components, respectively, and the '...' include higher order multipoles, skew components, and terms involving their z-derivatives.

Now, we "only" have to find the generalized gradients from the field data. To this end we have developed two companion programs, `computeCGGE` and `computeRGGE` [4] to compute the generalized gradient expansion (GGE) from the normal field data on a cylinder or rectangular prism, respectively. The former applies the algorithm of Ref. [2] while the latter follows that provided in [1]. The output is formatted for particle tracking with `elegant`'s [5] `BGGEXP` element. The `BGGEXP` element itself can compute the vector potential $\boldsymbol{A}$ from the GGE to symplectically integrate the trajectories using the implicit midpoint algorithm; alternatively, an explicit integrator is also available that sacrifices symplecticticity for speed.

We show examples of results obtained from simulated magnetic field data in Fig. 1. Panel (a) plots the on-axis quadrupole, dipole, and sextupole components obtained from APS-U's transverse gradient reverse bend Q4 dipole. The magnetic model was computed using `OPERA` and is described further in Ref. [6]. Figure 1(b) shows the on-axis dipole field for the A:M1 longitudinal gradient bend, along with the difference ΔB_y between the `OPERA` data and that predicted by the GGE. We see that the two agree to one part in $\sim 10^5$ for the body fields, and differ in the fringe regions between magnetic segments at the $\sim 10^{-3}$ level or better.

Similar GGE models were prepared using `OEPRA` data for the rest of the APS-U magnets, including an additional four

* Work supported by the U.S. Department of Energy, Office of Science, Office of Basic Energy Sciences, under Contract No. DE-AC02-06CH11357.

ISBN: 978-3-95450-232-5 ISSN: 2673-7000 doi:10.18429/JACoW-NAPAC2022-WEXD2

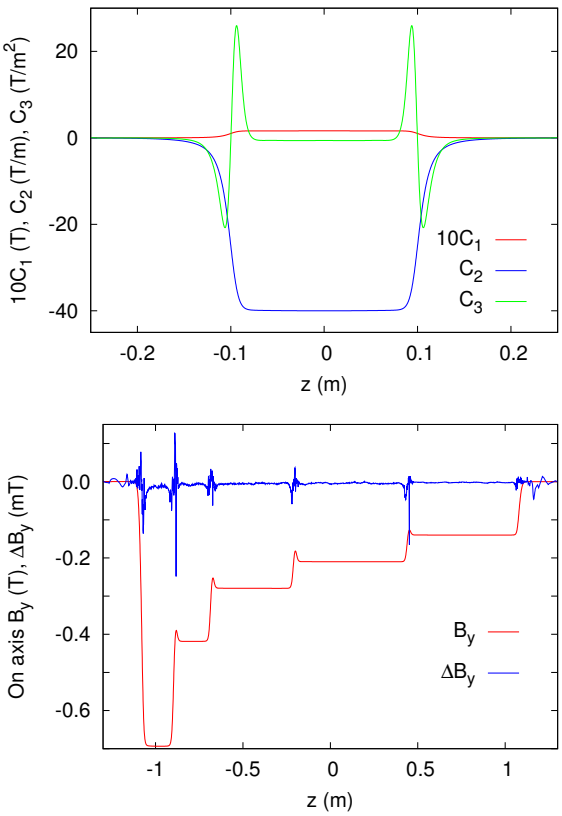

Figure 1: Examples of generalized gradient modeling of magnetic fields. (a) plots the on-axis dipole, quadrupole, and sextupole gradients for APS-U's Q4 transverse gradient reverse bend. (b) shows the on-axis B_y and the difference between the OPERA and the GGE for the A:M1 longitudinal gradient bend.

transverse gradient dipoles (Q5, Q8, M3, M4), an additional three longitudinal gradient dipoles (A:M2, B:M1, B:M2), five "normal" quadrupoles, and twelve flavors of sextupoles. These were then used to construct an "all GGE" lattice, whose properties we could compare to the more conventional lattice based upon hard edge models.

APS-U LATTICE TRACKING WITH GENERALIZED GRADIENTS

The APS-U uses a hybrid lattice design [7] with seven bends plus six reverse bends [8, 9] per sector to achieve a 42 pm natural emittance [10]. We build our GGE model of the APS-U lattice in two steps. First, we tuned each GGE element by scaling the fields and adjusting the positions to best match the first- and second-order properties of the corresponding hard edge element. Second, we applied global tuning to control the orbit and reproduce the linear optics and chromaticity. This two-step process relies on the numerical calculation of second order transport matrices [11] and their subsequent optimization. While somewhat laborious and computationally intensive, it is practical when when using parallel resources [12].

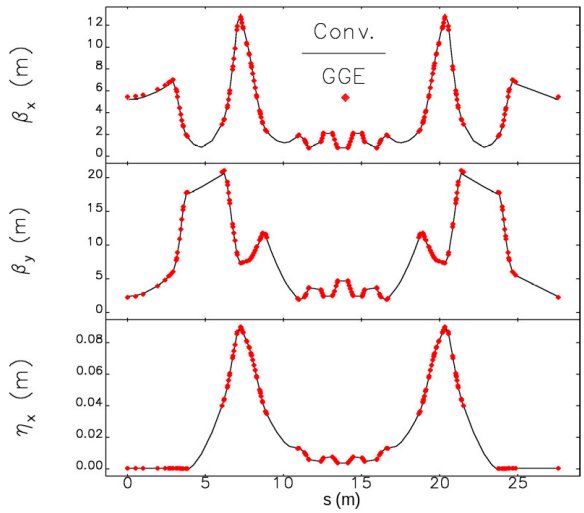

Figure 2: Comparison of the APS-U linear lattice functions as predicted by both conventional tracking and by the generalized gradient expansion (GGE). The good match was obtained after optimizing both the individual magnets and the global linear optics.

We compare the resulting GGE-based lattice functions with their conventional, hard edge counterparts in Fig. 2. We see that the predicted beta functions and the linear dispersion function agree very well.

Having matched the linear optics and linear chromaticity, we want to see to what extent the two models agree. We begin with the nonlinear chromatic tune dependance, since this is an important component of the momentum aperture and, hence, the lifetime. We compare predictions for GGE and conventional tracking for how the tune depends upon the momentum deviation δ in Fig. 3(a). The GGE tracking for ν_x in black closely matches the conventional tracking in green over the entire range $|\delta| \leq 5\%$; Significantly, they both cross the integer at the same point. The agreement between the two predictions for ν_y is also quite good. Figure 3(b) plots the tune footprint for $\delta \gtrsim 0.01\%$ where the predictions differ the most. Nevertheless, the agreement is still quite reasonable.

Next, we want to determine to what extent the resulting nonlinear dynamics match. We plot in Fig. 4(a) the dynamic acceptance predicted by both the traditional and GGE tracking. The shape and total area of the two predictions is nearly identical, while the traditional tracking predicts a slightly smaller horizontal acceptance and a slightly larger vertical acceptance.

We compare the nonlinear dynamics more closely in Fig. 4(b), where we compare the frequency map analysis between the two methods. In this case we find that while two predictions match in overall shapes and have some similar features for $y \gtrsim 1.5$ mm, the detailed resonance structure is rather different between the two methods. At this point we are unsure what the source of these discrepancies may be.

ISBN: 978-3-95450-232-5 ISSN: 2673-7000 doi:10.18429/JACoW-NAPAC2022-WEXD2

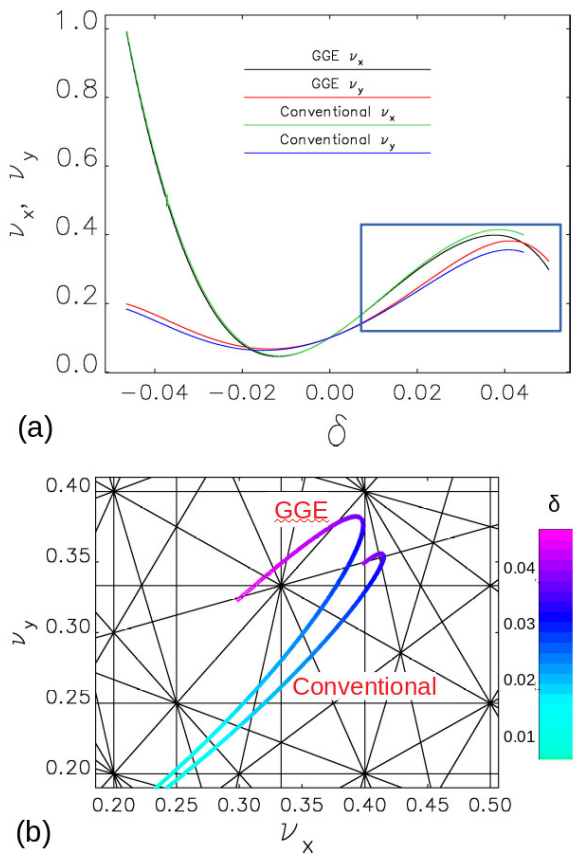

Figure 3: Comparison of the APS-U tune footprint between conventional tracking and that with the generalized gradient expansion (GGE). (a) plots the momentum dependence of the tunes for the two methods over the entire range, while (b) plots the tunes against each other for $\delta \gtrsim 0.01\%$ as indicated by the boxed region in (a).

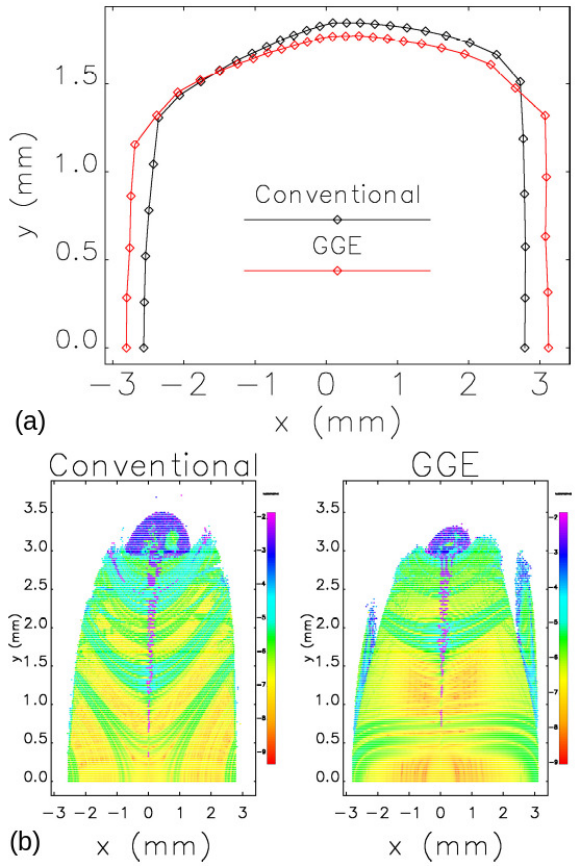

Figure 4: Comparison of the APS-U nonlinear dynamics between conventional tracking and that with the generalized gradient expansion (GGE). (a) plots the predicted dynamic acceptance of the two methods, while (b) compares the frequency map analysis.

Next, we try to assess to what extent the two models respond to lattice errors in similar ways. We do this by comparing how each model responds to randomly misaligning all the sextupoles by 30 microns rms. We plot the observed lattice beat amplitudes for β_x (top), β_y (middle), and η_x (bottom) in Fig. 5(a). We see good agreement between the two methods for the beat amplitude at each instance/index of random setupole errors. The average beating is plotted as the horizontal lines, which agree to better than 10%.

Figure 5(b) summarizes the resulting Touschek lifetimes from the error sets of Fig. 5(b). For this calculation we assumed that the APS-U reached its design values of $\varepsilon_x = \varepsilon_y = 30$ pm, $\sigma_\delta = 0.12\%$, and $\sigma_t = 100$ ps. In this case the conventional and GGE tracking predict nearly identical best and worst lifetimes, and agree to within 8% over the entire range.

Finally, we want to verify our calculations that relate the damping and diffusion due to synchrotron emission to the electron beam emittance and energy spread at equilibrium. Specifically, we will compare predictions based upon hard edge models to those obtained from both literal tracking using generalized gradients and the calculation of diffusion matrices. While there is no reason to believe that these models will differ, since the ultra-low emittance of 42 pm is a key performance parameter of the APS-U we think that the exercise is worth it.

To make this comparison we tracking 1k particles through 10k turns of the full GGE lattice of the APS-U, and then averaged the observed emittance and energy spread over the final 5k turns. We found a natural emittance $\varepsilon_{x,n} = 41.0$ pm, and an energy spread $\sigma_\delta = 0.0127\%$. These were essentially identical to predictions made using diffusion matrices calculated using the GGEs, which in turn were very close to hard edge predictions. Note, however, that the literal tracking used 48k core hours to complete, while calculating the diffusion matrices "only" required about 200 hours; the hard edge models need only a few seconds. Hence, we think that while this verification was worth it given how critical the emittance is to the APS-U's success, it is not something to undertake lightly.

We have found reasonably good agreement between lattice tracking with conventional and GGE models. Significantly, the big picture conclusions regarding dynamic acceptance, response to lattice errors, and lifetime remain unchanged,

ISBN: 978-3-95450-232-5 ISSN: 2673-7000 doi:10.18429/JACoW-NAPAC2022-WEXD2

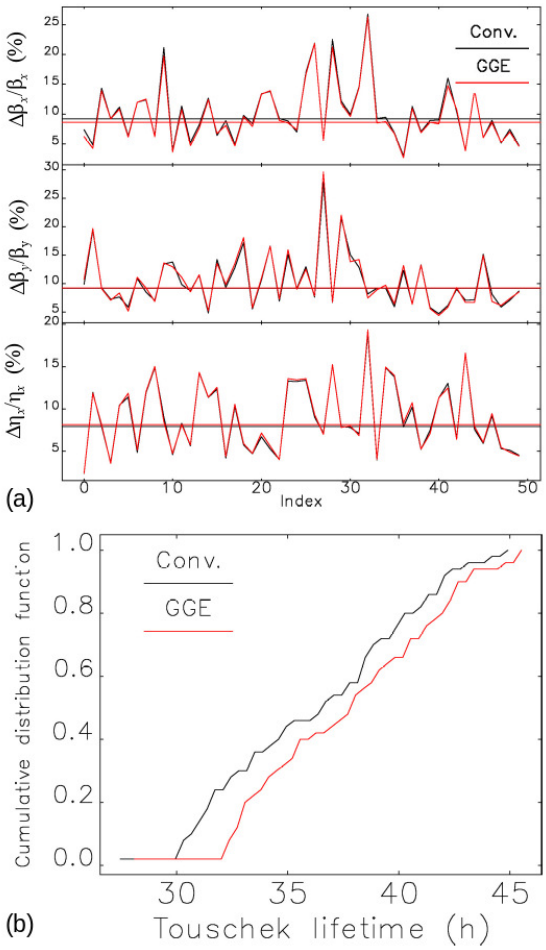

Figure 5: (a) Comparison of the observed latice function beating between conventional and GGE tracking. The agreement for each instance/index is very good, as is the average (horizontal lines). (b) plots their corresponding Touschek lifetimes assuming $\varepsilon_x = \varepsilon_y = 30$ pm, $\sigma_\delta = 0.12\%$, and $\sigma_t = 100$ ps.

even if some of the details may have differed. Nevertheless, these differences have indicated that some of the hard edge models could be improved. For example, matching the transverse gradient dipoles required adjustments of their quadrupole and dipole strength by a few percent, while matching the longitudinal gradient dipoles led to rather large ($\sim$ 2 mm) longitudinal displacements. This indicates that the perhaps a better hard edge model would lead to fewer adjustments and better detailed agreement. In the next section we summarize our work to improve the models for Cartesian bends, particularly those that include transverse and longitudinal gradients.

TRANSVERSE GRADIENT TRACKING: A REFERENCE FOR SIMPLIFIED MODELS

In this section we discuss using generalized gradient tracking as a "standard" by which to judge simplified magnet models. Specifically, we describe our efforts to develop

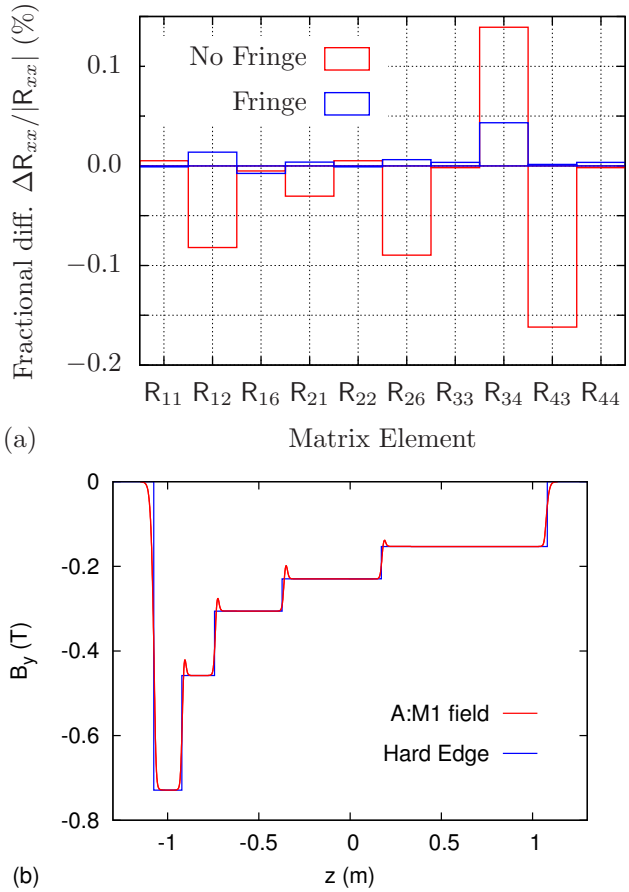

Figure 6: (a) Fractional difference from tracking with generalized gradients for the linear matrix elements of two hard edge model predictions for the Q4 transverse gradient reverse bend. (b) On axis profile B_y and its hard edge model for the A:M1 longitudinal gradient dipole.

improved hard edge models of the APS-U bends that have straight poles and include transverse or longitudinal gradients.

Our first goal is improve our model of the APS-U Q4 and Q5 magnets. These are transverse gradient reverse bends, with strong transverse focusing and relatively weak bending. The magnetic poles of the Q4 and Q5 are straight, so that the appropriate hard edge model in `elegant` is the `CCBEND` element [13] that integrates the motion in Cartesian xyz coordinates. We describe our hard edge model in Ref. [14]. In short, we define the magnet edges such that the integrated dipole field of the generalized gradient expansion matches that of the hard edge model, and then the quadrupole and higher-order multipole components are set by the corresponding GGE maxima values. Fringe field contributions are then introduced to account for the leading order difference between the hard edge and true field profile.

We compare the two hard edge models with the generalized gradient tracking in Fig. 6(a). Here, we plot the fractional difference in the transverse matrix elements, showing that the hard edge model matches to withing 0.15%, while adding the fringe field contributions improves the agreement

ISBN: 978-3-95450-232-5 ISSN: 2673-7000 doi:10.18429/JACoW-NAPAC2022-WEXD2

Table 1: Predicted linear lattice functions and natural chromaticities for the APS-U lattice when we replace the Q4, Q5, or Q4+Q5 transverse gradient reverse bends with either their GGE (BGGEXP) or hard edge (CCBEND) model.

Model	β_x (m)	β_y (m)	η_x (mm)	ν_x	ν_x	nat. ξ_x	nat. ξ_y
BGGEXP Q4	5.071	2.398	0.3507	94.986	36.088	−131.45	−111.79
CCBEND Q4	5.068	2.399	0.3471	94.983	36.087	−131.41	−111.79
BGGEXP Q5	5.220	2.406	0.3938	95.116	36.076	−133.95	−111.39
CCBEND Q5	5.219	2.406	0.3936	95.115	36.076	−133.94	−111.39
BGGEXP Q4+Q5	5.102	2.413	-0.6282	95.001	36.064	−132.09	−111.55
CCBEND Q4+Q5	5.085	2.414	0.4601	94.998	36.063	−131.68	−111.55

by almost an order of magnitude. It turns out that the hard edge model alone is not sufficient for good predictions of the APS-U linear optics: because the Q4 magnet has a relatively large beta function, the additional focusing results in a tune discrepancy of $\Delta\nu_x \approx 0.015$ and $\Delta\nu_y \approx 0.068$. As we show in Table 1, including fringe fields reduces the tune differences to ≤ 0.003 in both planes. The Table shows that these good results continue for the Q5 magnet, or if we model both Q4 and Q5.

Next, we would like to discuss how we used tracking with GGEs to verify a new hard edge model of the APS-U's A:M1 longitudinal gradient bend. In this case the field varies longitudinally over five magnetic segments as shown in Fig. 6(b). Again, we define the hard edges and field values to match the integrated B_y, and provide more details in [14]; the resulting approximation is plotted in blue in Fig. 6(b).

We summarize the fractional difference between the linear matrix obtained from GGE tracking and that of the LGBEND model as

$$\frac{\Delta R_{xx}}{R_{xx}}(\%) = \begin{bmatrix} -0.006 & -0.004 & 0 & 0 & 0 & -0.140 \\ 5.3 & -0.006 & 0 & 0 & 0 & -0.005 \\ 0 & 0 & 0.006 & 0.003 & 0 & 0 \\ 0 & 0 & 10.7 & 0.006 & 0 & 0 \\ -0.002 & 0.23 & 0 & 0 & 0 & 0.005 \\ 0 & 0 & 0 & 0 & 0 & 0 \end{bmatrix},$$

where, as noted, everything is the percent fractional difference. The two discrepancies that stand out are the 5.3% difference in R_{21} and the 10.7% difference R_{43}, but they are less troubling when we realize that the focusing in the A:M1 magnet was designed to be small, so that the the size of the elements themselves $R_{21} \approx -2R_{43} \approx -0.001$ 1/m. Hence, both models give very small contributions to the linear focusing in both plances, and nearly indistinguishable predictions of the linear lattice properties.

CONCLUSIONS

We have indicated how full magnetic field maps may be converted into a generalized gradient expansion suitable for symplectic tracking. These full-field magnet models may then be matched to form a full model of the lattice, and we showed how this lattice may then be used to verify predictions made with simpler models. We showed that the GGE predictions regarding the linear properties, the nonlinear perfomance, and response to errors is quite similar to those of the hard edge model. Hence, we feel confident in our modeling. Finally, we showed that GGE tracking can be used to improve the hard edge models.

REFERENCES

[1] A. J. Dragt, *Lie Methods for Nonlinear Dynamics with Applications to Accelerator Physics*. University of Maryland, 2009; https://www.physics.umd.edu/dsat/docs/Book19Nov2020.pdf

[2] M. Venturini and A. Dragt, "Accurate computation of transfer maps from magnetic field data," *NIM A*, vol. 427, pp. 387–392, 1999.

[3] C. E. Mitchell and A. J. Dragt, "Accurate transfer maps for realistic beam-line elements: Straight elements," *Phys. Rev. ST Accel. Beams*, vol. 13, p. 064001, 2010. doi:10.1103/PhysRevSTAB.13.064001

[4] M. Borland, R. R. Lindberg, R. Soliday, and A. Xiao, "Tools for Use of Generalized Gradient Expansions in Accelerator Simulations," in *Proc. IPAC'21*, Campinas, Brazil, May 2021, pp. 253–256. doi:10.18429/JACoW-IPAC2021-MOPAB059

[5] M. Borland, "elegant: A Flexible SDDS-Compliant Code for Accelerator Simulation," Tech. Rep. LS-287, Advanced Photon Source, September 2000.

[6] M. S. Jaski *et al.*, "Magnet Designs for the Multi-bend Achromat Lattice at the Advanced Photon Source", in *Proc. IPAC'15*, Richmond, VA, USA, May 2015, pp. 3260–3263. doi:10.18429/JACoW-IPAC2015-WEPTY003

[7] L. Farvacque *et al.*, "A Low-Emittance Lattice for the ESRF", in *Proc. IPAC'13*, Shanghai, China, May 2013, paper MOPEA008, pp. 79–81.

[8] J. Delahaye and J. P. Potier, "Reverse bending magnets in a combined-function lattice for the CLIC damping ring," in *PAC89*, pp. 1611–1613, 1990. doi:10.1109/PAC.1989.72869

[9] A. Streun, "The anti-bend cell for ultralow emittance storage ring lattices," *NIM A*, vol. 737, pp. 148–154, 2014. doi:10.1016/j.nima.2013.11.064

[10] M. Borland, T. G. Berenc, R. R. Lindberg, V. Sajaev, and Y. P. Sun, "Lower Emittance Lattice for the Advanced Photon

ISBN: 978-3-95450-232-5 ISSN: 2673-7000 doi:10.18429/JACoW-NAPAC2022-WEXD2

Source Upgrade Using Reverse Bending Magnets", in *Proc. NAPAC'16*, Chicago, IL, USA, Oct. 2016, pp. 877–880. doi:10.18429/JACoW-NAPAC2016-WEPOB01

[11] M. Borland, "A High-Brightness Thermionic Microwave Electron Gun," PhD thesis, Stanford University, Stanford, CA, USA, Rep. SLAC-402, 1991.

[12] Y. Wang and M. Borland, "Pelegant: A Parallel Accelerator Simulation Code for Electron Generation and Tracking," *AIP Conf. Proc.*, vol. 877, p. 241, 2006.

[13] M. Borland, "Symplectic Integration in elegant," Tech. Rep. LS-356, Advanced Photon Source, 2021.

[14] R. Lindberg and M. Borland, "Fringe Field Maps for Cartesian Dipoles with Longitudinal and/or Transverse Gradients," presented at NAPAC'22, Albuquerque, New Mexico, USA, Aug. 2022, paper TUPA26, this conference.